our attention on the Jacobi coordinates corresponding to the A-B_2 and B-AB arrangements and transformations of these by rotating the radial Jacobi coordinates. Numerical applications have been made for H_2O, O_3, and SO_2 showing that the SCF method gives good results when using those transformed Jacobi coordinate systems, which are, exactly or closely, normal or local systems. From the computational point of view, we have used the pointwise variational HEG method to solve the coupled SCF equations. This method allows us to easily evaluate the potential matrix elements required in the variational calculations and is very well suited for the SCF treatment of general, nonmultinomial potentials.

Acknowledgment. This work has been supported by La Comisiõn Interministerial de Ciencia y Tecnología (Madrid, Spain) under project PB 86-0411. A.B. acknowledges a FPI fellowship provided by Ministerio de Educaciõn y Ciencia.

Formation of Maleic Anhydride on a Vanadyl Pyrophosphate Surface. A Theoretical Study of the Mechanism

Birgit Schiøtt, Karl Anker Jørgensen,*

Department of Chemistry, Aarhus University, DK-8000 Aarhus C, Denmark

and Roald Hoffmann*

Department of Chemistry and Materials Science Center, Cornell University, Ithaca, New York, 14853-1301
(Received: June 19, 1990)

An analysis of the electronic structure of the vanadyl pyrophosphate surface and of the oxidation of 1,3-butadiene to maleic anhydride by molecular oxygen catalyzed by this surface is presented. The surface contains pairs of edge-sharing vanadium-oxygen octahedra. Each pair has two vanadyl groups, one pointing toward the bulk of the catalyst and the other one being free to interact with incoming molecules. The frontier orbitals of 1,3-butadiene are set up for an interaction with the oxygen in the vanadyl group in a [2+4]-like concerted mechanism forming a 2,5-dihydrofuran. The most favorable geometries of the adsorbed species are discussed from an analysis based on the extended Hückel approach. The activation of molecular oxygen on the surface is discussed. A comparison of two structures, η^1-superoxo and η^2-peroxo adsorbed dioxygen is presented. A mechanism for the oxygen transfer to 2,5-dihydrofuran is proposed involving an initial abstraction of a hydrogen in the 2-position from 2,5-dihydrofuran by the coadsorbed dioxygen species, leading to first a 2-hydroxy derivative followed by the formation of an asymmetric unsaturated lactone. The oxidation of the 5-position is suggested to take place in a similar way.

Understanding and control of the transfer of oxygen and other heteroatoms to and from organic and inorganic species is pursued in academic as well as in industrial research.[1] Among commercially feasible heterogeneously catalyzed reactions, the class of selective oxidations of hydrocarbons is very important. The process of allylic ammoxidation of propylene to acrylonitrile on various mixed metal oxides[2] is an important reaction and 4.3 million tons[3] of the nitrile are so produced per year worldwide. The epoxidation of ethylene to ethylene oxide on a silver surface[4] is also very used in the industry (5.8 million tons per year[3]). Generally, for these very important and useful reactions the underlying mechanisms of the selective oxidations are not well understood. Some theoretical investigations of acrolein production from propylene using a mixed molybdenum-bismuth oxide catalyst[5] and for the adsorbtion of ammonia on V_2O_5, an important step in the ammoxidation reaction,[2c] have been published. Several studies of ethylene epoxidation on a Ag(110) surface[6] have also appeared recently. Perhaps the most intriguing process among the heterogeneously catalyzed selective oxidation reactions is the synthesis of maleic anhydride from *n*-butane over a vanadium phosphorous oxide surface in the presence of molecular oxygen (eq 1).[7]

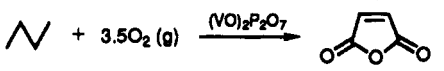

(1)

This reaction, being a 14-electron oxidation involving an abstraction of eight hydrogen atoms and an insertion of three oxygen atoms, has been the subject of a large number of reports[7,8] and will be the matter discussed in this paper.

The solid-state chemistry of the vanadium phosphorous oxide system is characterized by a large number of crystalline phases[9]

(1) (a) Sheldon, R. A.; Kochi, J. K. *Metal-Catalyzed Oxidations of Organic Compounds*; Academic Press: New York, 1981. (b) Holm, R. *Chem. Rev.* **1987**, *87*, 1401. (c) Jørgensen, K. A. *Chem. Rev.* **1989**, *89*, 431. (d) Nugent, W. A.; Mayer, J. M. *Metal-Ligand Multible Bonds*; Wiley Interscience: New York, 1988. (e) Meunier, B. *Bull. Soc. Chim. Fr.* **1986**, 578.

(2) (a) Burrington, J. D.; Grasselli, R. K. *J. Catal.* **1979**, *59*, 79. (b) Burrington, J. D.; Kartisek, C. T.; Grasselli, R. K. *J. Catal.* **1980**, *63*, 253; **1983**, *81*, 489; **1984**, *87*, 363. (c) Otamiri, J.; Andersson, A.; Jansen, S. A. *Langmuir* **1990**, *6*, 365.

(3) Grasselli, R. K. *J. Chem. Educ.* **1986**, *63*, 216.

(4) (a) Barteau, M. A.; Madix, R. J. In *The Chemical Physics of Solid Surfaces and Heterogenous Catalysis*; King, D. A., Woodruff, D. P., Eds.; Elsevier Scientific: New York, 1982; p 95. (b) van Santen, R. A.; Kuipers, H. P. C. E. *Adv. Catal.* **1989**, *35*, 265.

(5) Anderson, A. B.; Ewing, D. W.; Kim, Y.; Grasselli, R. K.; Burrington, J. D.; Brazdil, J. F. *J. Catal.* **1985**, *86*, 222.

(6) (a) Carter, E. A.; Goddard II, W. A. *J. Catal.* **1988**, *112*, 80; *Surf. Sci.* **1989**, *209*, 243. (b) Jørgensen, K. A.; Hoffmann, R. *J. Phys. Chem.* **1990**, *94*, 3046.

(7) (a) Centi, G.; Trifirò, F.; Ebner, J. R.; Franchetti, V. M. *Chem. Rev.* **1988**, *88*, 55. (b) Hodnett, B. K. *Catal. Rev.-Sci. Eng.* **1985**, *27*, 373.

(8) (a) Pepera, M. A.; Callahan, J. L.; Desmond, M. J.; Milberger, E. C.; Blum, P. R.; Bremer, N. J. *J. Am. Chem. Soc.* **1985**, *107*, 4883. (b) Busca, G.; Centi, G. *J. Am. Chem. Soc.* **1989**, *111*, 46. (c) Wohlfahrt, K.; Hofmann, H. *Chem.-Ing.-Tech.* **1980**, *52*, 811. (d) Kruchinin, Yu. A.; Mishchenko, Yu. A.; Nechiporuk, P. P.; Gel'bshtein, A. I. *Kinet. Katal. (Engl. Transl.)* **1984**, *25*, 328.

(9) (a) Tachez, M.; Theobald, F.; Bordes, E. J. *Solid State Chem.* **1981**, *40*, 280. (b) Torardi, C. C.; Calabrese, J. C. *Inorg. Chem.* **1984**, *23*, 1308. (c) Bordes, E.; Courtine, P. *J. Chem. Soc., Chem. Commun.* **1985**, 294. (d) Bordes, E.; Johnson, J. W.; Ramonosona, A.; Courtine, P.; *Proc. 10th Int. Symp. Reactivity Solids (Dijon, 1984)* Mater. Sci. Monogr. **1984**, *28B*, 887.

0022-3654/91/2095-2297$02.50/0

that easily interconvert upon reduction and oxidation.[7a,10] The active vanadium phosphorous oxide phase in the oxidation of *n*-butane has been disputed in the literature.[7a,9,10] Generally, it is agreed that the presence of the vanadyl pyrophosphate phase, $(VO)_2P_2O_7$, in the catalyst is necessary for the reaction to proceed.[11] An analysis of a commercially used vanadium phosphorous oxide catalyst showed only the presence of one crystalline phase by X-ray diffraction measurements, namely the vanadyl pyrophosphate phase.[7a] Furthermore, it revealed an oxidation state for vanadium of 4.00–4.03 and a P:V ratio of 1.00 ± 0.02,[7a] consistent with the assignment of $(VO)_2P_2O_7$ as the active phase. Most of the mechanistic studies are thus performed using a clean vanadyl pyrophosphate surface as the catalyst. Here also we will concentrate on this particular vanadium phosphorous oxide structure.

Vanadyl pyrophosphate has a layered structure. The layers consist of pairs of edge-sharing vanadium–oxygen octahedra linked together in the plane by pyrophosphate units, **1**. The planes are

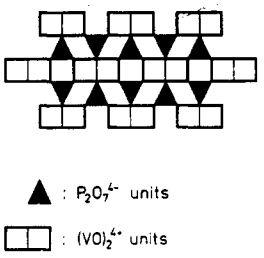

1

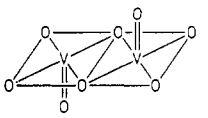

2

linked together through the axial oxygens of the edge-sharing octahedra. A tetragonal distortion of the octahedral environment of vanadium in the double chain direction is observed by the X-ray crystallographic investigations.[12] The two vanadyl groups hereby formed are placed trans to one another within one pair of edge-sharing vanadium octahedra, **2**. The interlayer bonding can be described as a weak Lewis acid → Lewis base interaction (V=O → V=O).[8a]

It is very important to obtain knowledge about the structure of the surface of a $(VO)_2P_2O_7$ crystal in order to trace a likely mechanism for the selective oxidation of *n*-butane to maleic anhydride. Satsuma et al. have described the surface structure in terms of the number of surface V=O groups and surface acid sites, using various physical and chemical methods.[13] They were able to show that the vanadyl group, V=O, is presented to a large extent on the surface of vanadyl pyrophosphate. The surface acid sites were identified as Brønsted acid sites, such as P–OH, whereas a small number of Lewis acid sites were found associated to the surface vanadium atoms. In this study we will apply one layer of the vanadyl pyrophosphate structure as a model for the active surface. One vanadyl dimer contains both the surface V=O unit and a Lewis acid site, namely at the vanadyl group pointing toward the bulk.

The rate-determining step in the oxidation of butane on a vanadyl pyrophosphate surface has been shown to be the activation of the methylene carbon–hydrogen bond(s).[8a,14] In order to trace the steps of the reaction that are responsible for the large selectivity to maleic anhydride, the oxidation of thereby formed unsaturated species, such as 1-butene and 1,3-butadiene, has been very intensively studied.[11c,15] For these species the rate-controlling step toward maleic anhydride is the insertion of oxygen into the hydrocarbon.[15a] This is very different from other olefinic selective oxidations, as, for example, the propylene to acrolein synthesis.[2]

SCHEME I

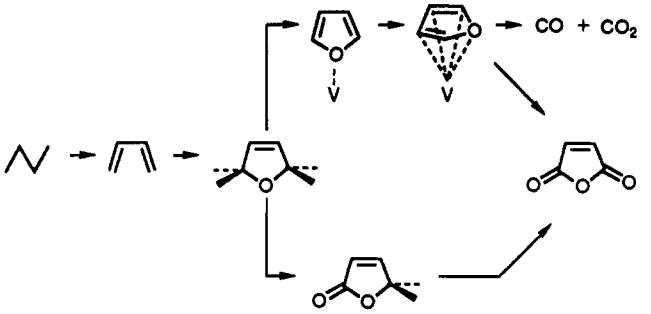

Concerning the oxygen source for the maleic anhydride reaction, it also differs from other selective oxidation reactions. Usually, the bulk of the catalyst is involved in the oxidation of the organic fragment by undergoing a reduction in the promotion of oxygen to the active surface.[16] In the formation of acrolein from propylene on a mixed molybdenum–bismuth oxide surface, gas-phase oxygen is not an absolute necessity for the product formation.[2,17] For this reaction it has been shown by labeling studies that bulk oxygen atoms are transferred to the hydrocarbon.[17] In the case of vanadyl pyrophosphate, bulk oxygens are not involved in the reaction[18] and only small amounts of maleic anhydride are formed in the absence of $O_2(g)$.[7a,8a,b] The main product of 1-butene oxidation in the absence of $O_2(g)$ on $(VO)_2P_2O_7$ was thus crotonaldehyde, obtained by an oxydehydrogenation and an allylic oxidation.[15b]

How the molecular oxygen becomes activated at the vanadyl pyrophosphate surface, and in which form (gas phase, physisorbed, or surface lattice) it becomes incorporated into the products, are still unanswered and disputed questions.[7,8] It has been rationalized that the vanadyl pyrophosphate surface can adsorb one oxygen molecule per two surface vanadium atoms.[8a] Also, by using butadiene as starting material, Centi and Trifirò were able to show that the furan–oxygen is introduced through an attack of an electrophilic oxygen on the 1,4-positions of butadiene to give 2,5-dihydrofuran.[15a] Recently, Busca and Centi[8b] detected at least three different intermediates besides the 2,5-dihydrofuran, namely an unsaturated lactone and two structures of adsorbed furan. Two competing reaction paths could be distinguished, as shown in Scheme I. There is postulated a fast path, involving an asymmetric unsaturated lactone (lower reaction path) and a slower one, passing through a furan intermediate (upper reaction path). The slow path was shown to be the less selective way, giving rise to the formation of CO and CO_2.[8b]

In this study we will focus on the lower and more selective path. The "upstanding" O-coordinated form of adsorbed furan is more stable by ~2–3 eV than the "lying down" π-coordinated form, depicted in the upper path. An analysis of the bonding situation between a vanadyl pyrophosphate surface and the various adsorbates (butadiene, 2,5-dihydrofuran, and the lactone) is made in order to trace the most likely adsorption geometry of these intermediates. The nature of the active oxygen is also discussed and a mechanism for the selective oxygen transfer is proposed. Throughout the study the extended Hückel[19] approximation is used. Due to limitations in computational time a cluster model is applied for the more complex structures; otherwise tight binding[20] calculations are performed. Further details of the

(10) Johnson, J. W.; Johnston, D. C.; Jacobson, A. J.; Brody, J. F. *J. Am. Chem. Soc.* **1984**, *106*, 8123.
(11) (a) Bordes, E.; Courtine, P. *J. Catal.* **1979**, *57*, 236. (b) Cavani, F.; Centi, G.; Trifirò, F. *Appl. Catal.* **1984**, *9*, 191. (c) Centi, G.; Manenti, I.; Riva, A.; Trifirò, F. *Appl. Catal.* **1984**, *9*, 177. (d) Johnston, D. C.; Johnson, J. W. *J. Chem. Soc., Chem. Commun.* **1985**, 1720.
(12) Gorbunova, Yu. E.; Linde, S. A. *Sov. Phys. Dokl.* (*Engl. Transl.*) **1979**, *24*, 138.
(13) Satsuma, A.; Hattori, A.; Furuta, A.; Miyamota, A.; Hattori, T.; Murakami, Y. *J. Phys. Chem.* **1988**, *92*, 2275.
(14) Busca, G.; Centi, G.; Trifirò, F. *Appl. Catal.* **1986**, *25*, 265.
(15) (a) Centi, G.; Trifirò, F. *J. Mol. Catal.* **1986**, *35*, 255. (b) Morselli, L.; Trifirò, F.; Urban, L. *J. Catal.* **1982**, *75*, 112.
(16) (a) Krenzke, L. D.; Keulks, G. W. *J. Catal.* **1980**, *61*, 316. (b) Brazdil, J. F.; Suresh, D. D.; Grasselli, R. K. *J. Catal.* **1980**, *66*, 347. (c) Glaeser, L. C.; Brazdil, J. F.; Hazle, M. A.; Mehecic, M.; Grasselli, R. K. *J. Chem. Soc., Faraday Trans. 1* **1985**, *81*, 2903. (d) Mars, P.; van Krevelen, D. W. *Chem. Eng. Sci.* (*Spec. Suppl.*) **1954**, *3*, 41.
(17) Ueda, W.; Moro-oka, Y.; Ikawa, T. *J. Chem. Soc., Faraday Trans. 1* **1982**, *78*, 495.
(18) Buchanan, J. S.; Sundrasan, S. *Appl. Catal.* **1986**, *26*, 211.
(19) (a) Hoffmann, R. *J. Chem. Phys.* **1963**, *39*, 1397. (b) Hoffmann, R.; Lipscomb, W. N. *J. Chem. Phys.* **1962**, *37*, 2872.

TABLE I: Electronic Properties for the Different Models Used for the Vanadyl Pyrophosphate Surfaces with Vanadium in a +4 Oxidation State

	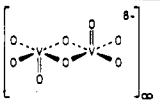	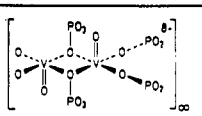	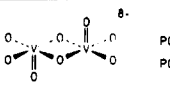	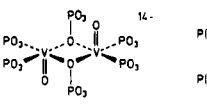	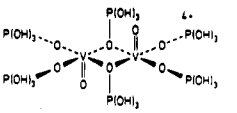
charge on V	1.95	2.03	2.03	2.14	2.20
charge on double bound O	−1.26	−1.26	−1.26	−1.26	−1.26
av charge of P		2.63		2.69	2.60
overlap populations					
V–V	0.010	0.039	0.010	0.041	0.042
V=O	0.758	0.767	0.761	0.773	0.771

TABLE II: Electronic Properties for the Different Models Used for the Vanadyl Pyrophosphate Surfaces with Vanadium in a +5 Oxidation State

	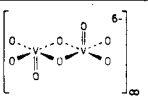	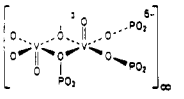	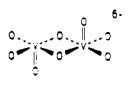
charge on V	2.92	3.01	2.91
charge on double bound O	−1.26	−1.26	−1.26
av charge of P		2.63	
overlap populations			
V–V	−0.037	0.039	0.010
V=O	0.758	0.767	0.761

calculations are given in the Appendix.

The Surface of Vanadyl Pyrophosphate

Let us start with an analysis of the clean vanadyl pyrophosphate surface. Although the structure of the surface is disputed in the literature,[7a,9,10] we will here limit ourselves to the (020) plane of $(VO)_2P_2O_7$ as the active surface.[7a,14] It has been proposed that the active sites are located at interfaces between different crystal phases.[9c] Though a crystal of one phase only, the vanadyl pyrophosphate phase serves well as a catalyst for the selective oxidation of *n*-butane to maleic anhydride.[8] Surface-sensitive experiments conclude that vanadyl, V=O, sites are found at the surface of a $(VO)_2P_2O_7$ crystal and also that surface Lewis acid sites are found.[13] One pair of edge-sharing VO_5 units contains both of these functional groups, **3**.

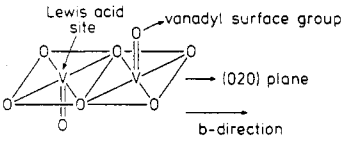

3

The surface of V_2O_5 has been analyzed theoretically.[2c] The structure of V_2O_5 consists also of tetragonally distorted edge-sharing octahedra. Because of the highly ionic structures for V_2O_5 and $(VO)_2P_2O_7$ the bonding within both structures is relatively localized, though some differences in the shape of the DOS (density of states) curves and in the atomic charges of the surface layer are computed which may account for their different reactivities.[2c,13,15b]

Due to limitations in computational time we will only use one layer of the vanadyl pyrophosphate structure as a model for the active surface. Usually, in the case of metal single-crystal surfaces three layers or more are recommended,[21] but for more ionically bonded, therefore localized, systems a one-layer model has been applied successfully as, e.g., in the analysis of the adsorption of organorhodium compounds on a rutile surface.[22] The unit cell within one (020) plane of vanadyl pyrophosphate is rather large, due to the alternating orientations of the pyrophosphate, $P_2O_7^{4-}$, groups. To avoid this enormous unit cell we make a one-dimensional approximation. In the following we will compare characteristic features of two one-dimensional chains made from pairs of edge-sharing VO_5 units. The dimension taken into account is the one along the *b* direction of the unit cell, meaning along the direction of the edge-sharing vanadyl groups. The first model consists of the bare vanadyl units, **4**. The second structure applied

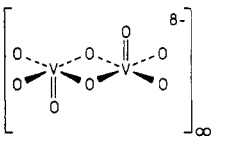

4

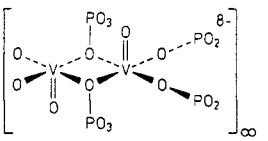

5

attaches PO_3 units as models for the pyrophosphates, **5**. The charge of each structural unit is chosen so as to given vanadium an oxidation state of +4 (all oxygens are in the −2 oxidation state), as is the case for the vanadium atoms in the vanadyl pyrophosphate structure.

Small defects in the $(VO)_2P_2O_7$ structure give rise to a small quantity of V^{5+} centers.[7a] Some authors have attributed to these the large selectivity for maleic anhydride.[7,15b,23] A calculation with vanadium in the oxidation state +5 is thus performed in order to investigate how the oxidation state can influence the adsorption processes regarded.

The distance between two nearest oxygens from two neighboring unit cells is rather large (the average oxygen–oxygen separation within a pyrophosphate unit is 2.50 Å[12]) so we expect very little inter unit cell interactions. For this reason we did molecular calculations on the parent compounds to the two chains. A calculation with $P(OH)_3$ units as models for the pyrophosphates, **6**, was also carried out for the +4 oxidation state of vanadium.

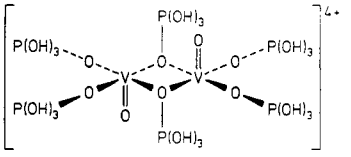

6

Important results are listed in Table I for the calculations with vanadium in a +4 oxidation state and in Table II for an oxidation state of +5.

For both oxidation states considered, the different models used to mimic the real surface gives consistent results. For the set of calculations with vanadium in the +4 oxidation state, all models give a net charge on vanadium of approximately +2.0 and of −1.26 for the double bound oxygens. Also, the vanadium–vanadium (V–V) overlap population is computed to be small and positive in all models. The overlap population of the vanadium–oxygen double bond is also almost unchanged from one model to the other, varying from 0.758 to 0.771.

(20) Whangbo, M.-H.; Hoffmann, R. *J. Am. Chem. Soc.* **1978**, *100*, 6093.
(21) Saillard, J.-Y.; Hoffmann, R. *J. Am. Chem. Soc.* **1984**, *106*, 2006.
(22) Halet, J.-F.; Hoffmann, R. *J. Am. Chem. Soc.* **1989**, *111*, 3548.
(23) Cavani, F.; Centi, G.; Trifirò, F. *Appl. Catal.* **1985**, *15*, 157.

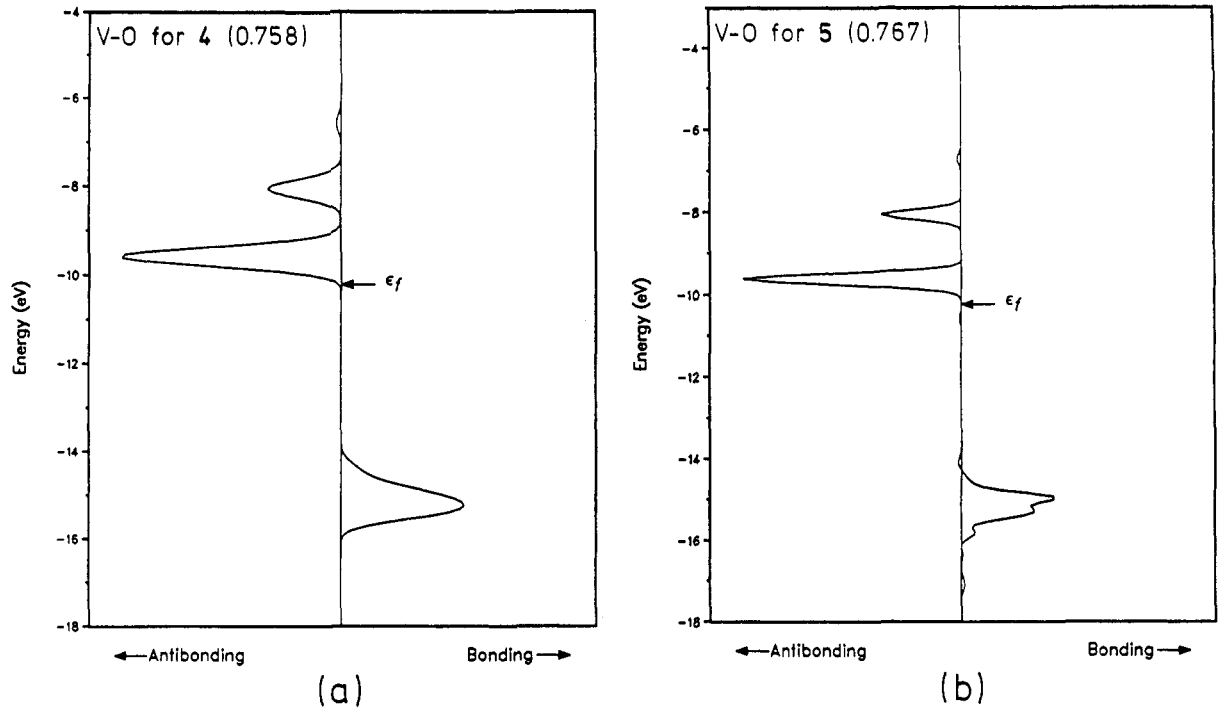

Figure 1. Crystal orbital overlap population (COOP) for the V=O bond in **4** (a) and **5** (b).

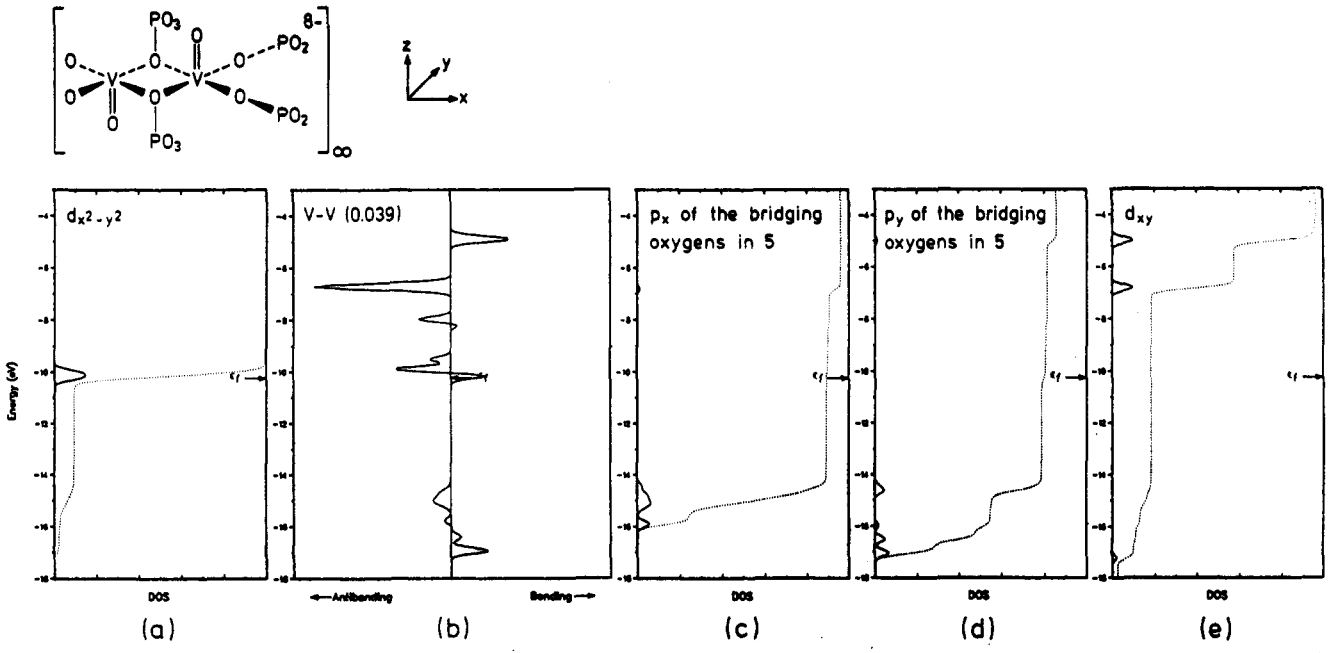

Figure 2. Some projected density of states (DOS) for structure **5**. (a) Contribution from the vanadium $d_{x^2-y^2}$ orbital to the total density of states. (b) Vanadium–vanadium COOP curve. (c) Contribution from the p_x orbitals of the bridging oxygens. (d) p_y orbitals of the bridging oxygens. (e) The projected density of states of the vanadium d_{xy} orbitals. Dotted lines give the integration of the depicted orbital.

The other set of calculations with two electrons less, giving vanadium in the +5 oxidation state, also comes out with consistent numbers for the characteristics listed. The charge on vanadium is about +3.0 in all three models. The overlap population of the vanadium–oxygen double bond remains unchanged compared to the calculations for the +4 oxidation state. The V–V overlap population has now settled on a small negative value.

The consistency between the models used is also found in the V=O COOP[24] (Crystal Orbital Overlap Population) curves for **4** and **5**, as seen in Figure 1, a and b, respectively. Both have a bonding peak at ~−15 eV and two peaks contributed by orbitals with antibonding V=O character above the Fermi level at ~−9.5 and −8.0 eV. The fine structure of the peaks is different because of the changed environment, but the main features remain the same. We will discuss below the origin of these features.

The removal of two electrons from the system by going from the +4 oxidation state of vanadium to the +5 oxidation state is accompanied by a decrease in the small V–V overlap population and an increase in positive charge located on each vanadium. These observations can be rationalized by an analysis of some DOS[24] and COOP curves. Some plots for structure **5** are shown in Figure 2 to explain the sign and magnitude of the V–V overlap population calculated.

The Fermi level of **5** is located at −10.2 eV. The plot shown in Figure 2a is the contribution from the vanadium $d_{x^2-y^2}$ orbitals to the total DOS. We see that ~10% of the states are found in the −14.5 to −17.0 eV range. These states cause a bonding and

(24) (a) Hoffmann, R. *Solids and Surfaces. A Chemists View of Bonding in Extended Structures*; VCH Publishers: New York, 1988. (b) Hoffmann, R. *Rev. Mod. Phys.* **1988**, *60*, 601. (c) Hoffmann, R. *Angew. Chem., Int. Ed. Engl.* **1987**, *26*, 846.

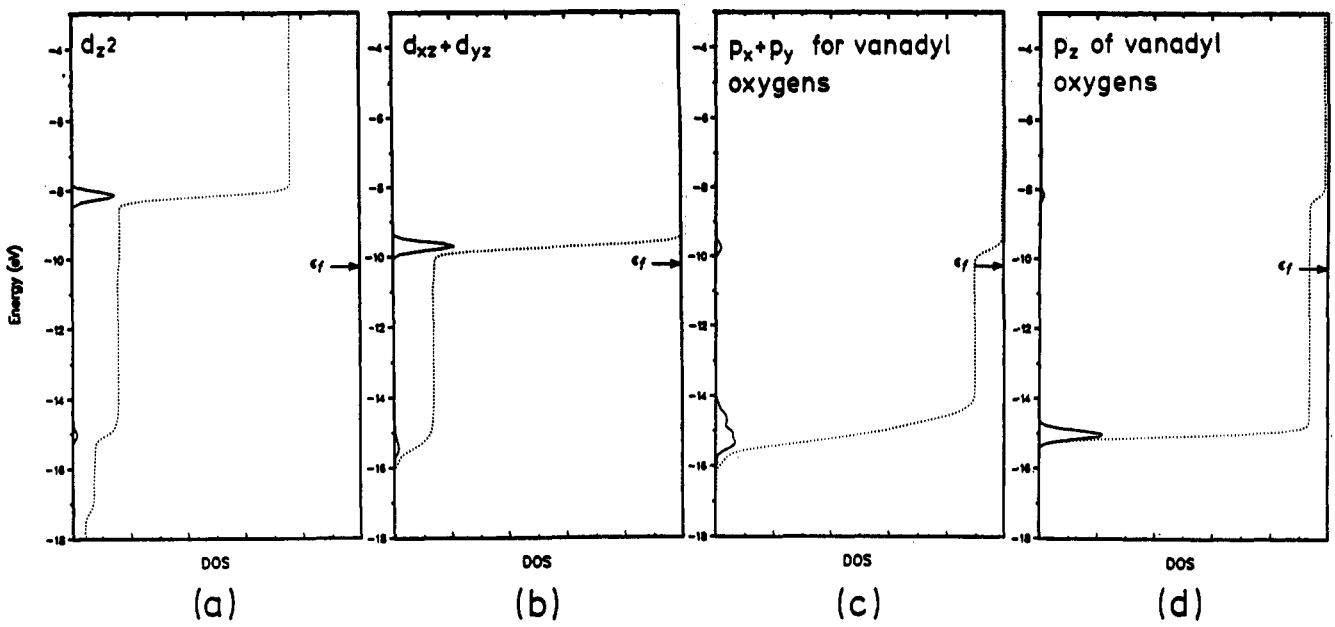

Figure 3. Projected density of states illustrating the V=O bonds in **5**. (a) Projected density of states of the vanadium d_{z^2} orbitals. (b) Contribution of the vanadium d_{xz} and d_{yz} orbitals to the total DOS. (c) Projected density of states of p_x and p_y from the vanadyl oxygens. (d) p_z of the vanadyl oxygens. Dotted curves give the integration of the projected DOS.

an antibonding peak in the V–V COOP curve, as depicted in Figure 2b. The antibonding peak is larger in magnitude than the bonding one, so the total V–V overlap population contributed by these lower peaks is negative, as calculated for the +5 oxidation state structures. The major part (90%) of the $d_{x^2-y^2}$ states is located around the Fermi level. These states also create a bonding and an antibonding V–V peak in the COOP. The Fermi level cuts at an energy halfway through this bonding peak explaining the small positive overlap population. This indicates only a small coupling of the d electron located at each vanadium center in agreement with the identification of a triplet ground state by EPR measurements.[8a] By going to the +5 oxidation state of vanadium two electrons are removed form each structural unit. A loss of 0.96 electrons for each $d_{x^2-y^2}$ is computed. The Fermi level, located at −10.7 eV, is now far below the upper V–V bonding peak, justifying the decrease in V–V overlap population.

The appearance of two peaks in the DOS for $d_{x^2-y^2}$ is a consequence of mixing with the p orbitals of the bridging oxygens. The DOS for p_x and p_y are plotted in Figure 2, c and d. We see a large contribution in the −14.0 to −17.5 eV range and a smaller one (~5%) around the Fermi level. A schematical drawing of the interaction of $d_{x^2-y^2}$ with the p_x and p_y of the bridging oxygens is shown in **7**. The $d_{x^2-y^2}$ orbitals of the two vanadium atoms

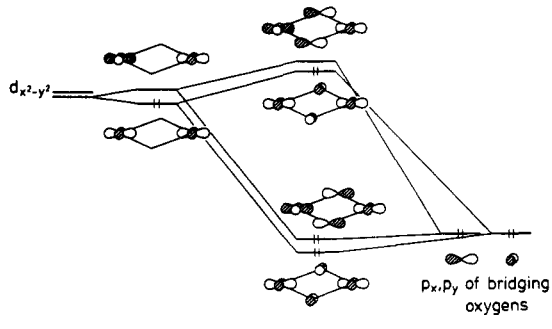

7

interact weakly, giving a bonding and an antibonding combination. Each of these interact with the p orbital of the bridging oxygens with the right symmetry. The four combinations obtained thereby explain the variations observed in the V–V COOP curve.

The bonding and antibonding combinations of the vanadium d_{xy} orbitals interact in a similar way with p_x and p_y of the bridging oxygens. The DOS for d_{xy} is plotted in Figure 2e. Two major peaks are found above the Fermi level at −5.0 and −6.8 eV. These are seen in the V–V COOP (Figure 2b) as a bonding, **8**, and an antibonding peak, **9**.

8 9

Figure 3 displays some important plots for the understanding of the vanadium–oxygen double bond. Figure 1b showed the COOP of the bond in question. Bonding states are found from −14 to −16 eV and the antibonding states are located above the Fermi level with two major peaks at −9.5 and −8.0 eV. The vanadium orbitals involved in this bonding are depicted in Figure 3a (d_{z^2}) and in Figure 3b (d_{xz}, d_{yz}). The bonding states are made up of interactions of d_{xz} and d_{yz} on the metals with p_x and p_y of the oxygens and of d_{z^2} with oxygen p_z and s. The antibonding peaks are easily distinguished with help from the DOS's. In Figure 3b the −10.0-eV peak just above the Fermi level is the antibonding π-type interaction, **10**, whereas the stronger σ interaction has its antibonding peak at a higher energy, −8.0 eV, **11** (Figure 3a). No

10 11

vanadium–oxygen states, bonding or antibonding, are located right below the Fermi level explaining the unaffected V=O overlap population when the oxidation state of vanadium is changed.

The numbers listed in Table I and II indicated only minor variations in the characteristics of the surface between the various models applied for the surface of vanadyl pyrophosphate. Extended models as well as discrete clusters, with and without phosphorous groups attached, all give very similar pictures of the electronic features for the vanadium and the oxygen atoms within the surface layer of $(VO)_2P_2O_7$. The above analysis of the extended surface models also reveals a great similarity with the bonding picture obtained from cluster models. These observations indicate that the simple surface model, a $V_2O_8^{8-}$ cluster, can as well explain the major trends in the formation of maleic anhydride on the vanadyl pyrophosphate surface as can an extended complex surface model, for which the calculations are slow and more expensive and the decomposition of the DOS's and COOP's are complicated.

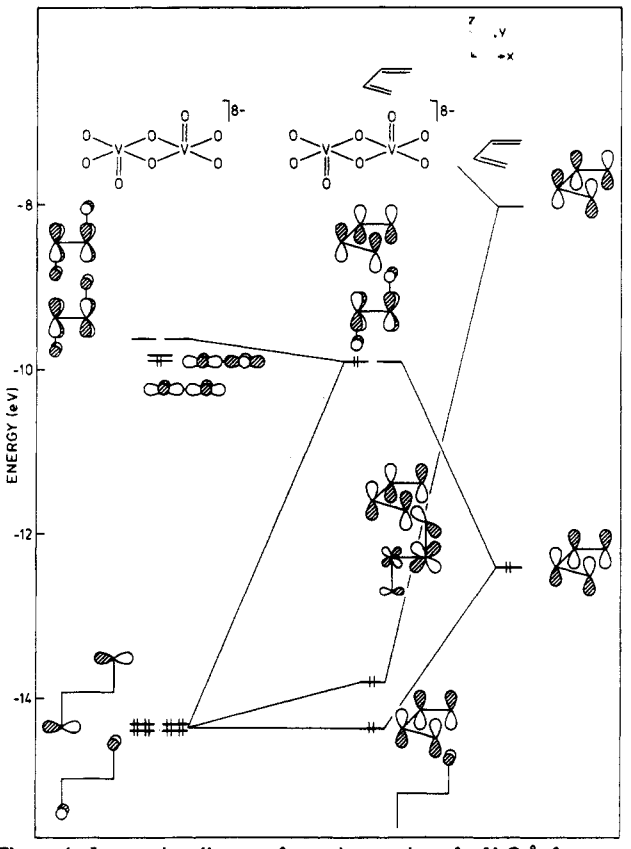

Figure 4. Interaction diagram for an interaction of a $V_2O_8^{8-}$ fragment (left) with 1,3-butadiene (right).

In the following we will focus on the oxygen transfer from the vanadyl pyrophosphate surface to butadiene. The hydrogen activation and abstraction steps going from *n*-butane to butadiene will not be considered in this study. Experimentally, it is believed that butadiene and *n*-butane pass through the same intermediates on the way to maleic anhydride, the first intermediate being 2,5-dihydrofuran.[7a,8]

The Formation and Bonding of 2,5-Dihydrofuran

It has been proposed that the furan oxygen is introduced through an attack of an electrophilic oxygen at the 1,4-positions of butadiene.[15a] This statement is in agreement with a simple orbital interaction diagram between the V=O group of the $(VO)_2O_6^{8-}$ cluster and butadiene, as shown in Figure 4. The oxygen–carbon distance is set to 1.60 Å, and the 1,4-positions of butadiene are at the same *x*-coordinate as the V=O unit of the surface. The left-hand side shows the frontier orbitals of $(VO)_2O_6^{8-}$. We recognize the bonding and antibonding combinations of the vanadium $d_{x^2-y^2}$ orbitals as the HOMO and LUMO, nearly degenerate in this molecular calculation. Right above the LUMO are located antibonding combinations of d_{xz} and d_{yz} with p_x and p_y, as in the one-dimensional calculations. These V–O antibonding orbitals are electrophilic in character when interacting with the HOMO of butadiene.

A decrease in overlap population for the vanadium–oxygen double bond from 0.761 to 0.495 is computed, verifying that a substantial fraction of V=O antibonding orbitals becomes populated upon adsorption. A decrease in overlap population for the carbon–carbon double bonds after adsorption is see too, from 1.465 to 1.137, due to a depletion of 0.67 electrons from the HOMO and a donation of 0.19 electrons to the LUMO of butadiene. A vertically oriented butadiene is also suitable for interaction with the vanadyl oxygen, but the energy of the product is disfavored by ~3 eV compared to the geometry shown in the center of Figure 4. The product of this [4+2] type reaction rearranges to the 2,5-dihydrofuran structure. We have examined some different orientations of 2,5-dihydrofuran (DHF) in order to trace a likely orientation of the intermediate in the maleic anhydride synthesis.

TABLE III: Total Energies and Some Overlap Populations for 14 and 15

	14	15
total energy, eV	−3253.1	−3252.8
overlap populations		
V=O	0.761	0.762
$V-O_{DHF}$	0.310	0.306
C–O	0.495	0.495

Four orientations of DHF adsorbed on a $(VO)_2O_6^{8-}$ cluster were tried. Two calculations with the DHF ring oriented parallel to the surface, **12**, and two calculations with the DHF ring perpendicular to the surface plane, **13**, were carried out. From an

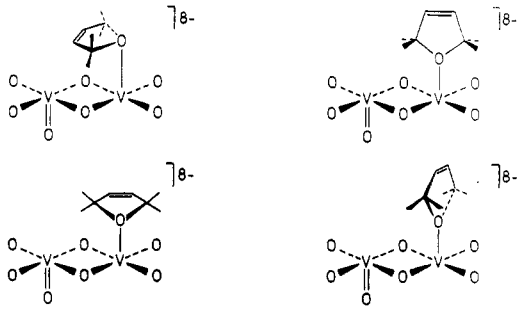

12 13

energetic point of view the two structures **12** are disfavored by 7 and 9 eV, respectively, compared to **13**, and they will not be considered further in this study. No energy minimum was found between the two limits shown in **12** and **13**. The two "upstanding" forms give similar energies. Calculations for these structures were carried out on the simple one-dimensional surface, **5**, to reveal whether or not a preference in the orientation of DHF could be found. Table III lists some results for the two structures examined, **14** and **15**. Very similar numbers are computed, though the

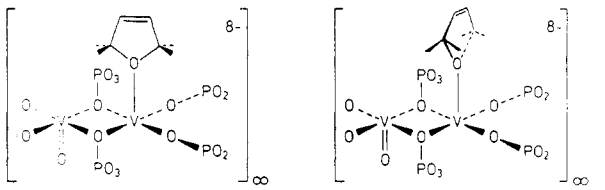

14 15

structure with the ring along the V–V direction, **14**, is slightly more favorable by 0.3 eV.

From these calculations it is concluded that DHF on a vanadyl pyrophosphate surface takes an upright position, but no specific conformation for this orientation can be picked as the most favorable.

Let us now proceed to a description of the bonding situation between DHF and the vanadyl pyrophosphate surface. For this purpose a one-dimensional chain of $(VO)_2O_6^{8-}$ is applied. The distance between the oxygen of DHF and vanadium is arbitrarily set to 2.0 Å.[25] Figure 5 displays some plots to examine the V–O and the C–O of **16**. Figure 5a is the COOP curve for the V–O

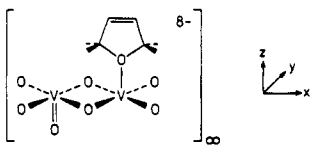

16

bond. Compared to Figure 1a, especially the bonding part has changed by splitting into many separated peaks. The orbitals that

(25) Mimoun, H.; Chaumette, P.; Mignard, M.; Saussine, L. *New J. Chem.* **1983**, *7*, 467.

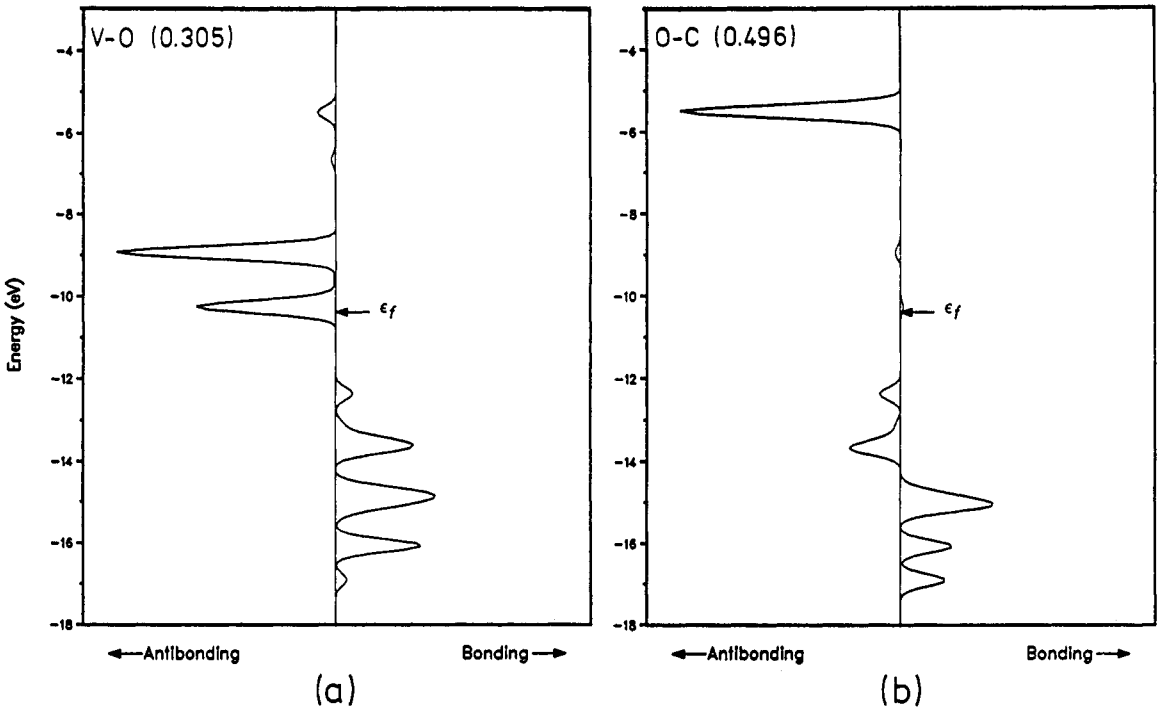

Figure 5. Some COOPs for the adsorption of DHF on the surface. (a) The COOP curve for the vanadium–oxygen double bond. (b) COOP for the carbon–oxygen bonds.

TABLE IV: Total Energies and Some Overlap Populations for 18 and 19

	18			
	θ = 180°	θ = 150°	θ = 90°	19
total energy, eV	−1524.5	−1524.7	−1521.5	−1524.2
overlap populations				
V=O[a]	0.720	0.721	0.721	0.697
O–O[b]	0.395	0.395	0.391	0.413

[a] V=O overlap population for the vanadium atom with O_2 coordinated. [b] The O–O overlap population of O_2(g) is 0.570.

make up the five bonding V–O peaks also have either O–C bonding or antibonding character as seen from the O–C COOP in Figure 5b. The DOS curves (not shown here) reveal that the four smallest (in amplitude) occupied peaks in the two COOP curves are made up from an interaction of the low-lying antibonding V–O π_x orbitals with the p_x on the 2,5-carbons of DHF. The two lower peaks are the bonding combinations, **17a**, and the upper ones are the antibonding ones resulting in no net P_x-type bonding between oxygen and carbon in the DHF ring. The major peak around

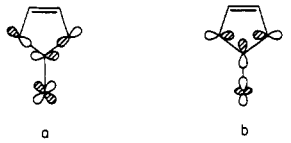

17

~−15 eV consists of the σ-type bonding orbitals, **17b**. The corresponding antibonding orbitals are located above the Fermi level. Again, the orbital picture obtained from a one-dimensional calculation is consistent with the cluster calculation. From Figure 5a it is seen that the Fermi level cuts at an energy halfway through a strongly antibonding V–O band. For the structure with two electrons less, vanadium in the +5 oxidation state, a higher V–O overlap population is thus calculated.

Activation of O_2(g) on the Vanadyl Pyrophosphate Surface

Bulk oxygens are not involved in the maleic anhydride formation from *n*-butane.[7a,8] Only lattice oxygens from the very outermost layers are transferred.[8d] The activation and incorporation of molecular oxygen into the vanadyl pyrophosphate surface is essential for keeping the large selectivity for maleic anhydride. Pepera et al.[8a] have showed that one oxygen molecule can be adsorbed per two surface vanadium centers. Within our model this could be one O_2 molecule per pair of edge-sharing vanadyl groups. An oxygen molecule can coordinate in two ways to one transition metal center,[26] as either a η^1-superoxo compound, **18**, or in the η^2-coordinated (peroxo) way, **19**. The bending angle,

18 19

θ, of the known superoxo complexes varies from ~115° to ~170°.[26] The oxygen–oxygen separation in **18** varies from 1.1 to 1.35 Å.[26] To our knowledge only structures with a peroxo-coordinated dioxygen has been reported for vanadium.[27] These show O–O distances of 1.41–1.47 Å.[27] In this study we will not consider dissociation of O_2 to O_{ads} because activation of DHF with O_{ads} will require this to migrate on the surface (shortest possible O–H separation between DHF and a neighboring vanadyl oxygen is ~1.7 Å) and extended Hückel is not a good method for this type of calculations. Table IV contains some results for η^1 and η^2-coordinated dioxygen to a chain of $(VO)_2O_6^{8-}$ units, **20**. Three

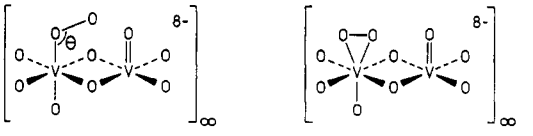

20

bending angles of the superoxo structure were used.

The separation of vanadium and one oxygen of the dioxygen fragment was taken to be 1.90 Å.[27] The oxygen–oxygen distance was set to 1.40 Å, as a compromise between the experimentally found distances for **18** and **19**.[27] The extended Hückel method does not allow comparison of overlap populations calculated for different bond lengths, and therefore, this necessity for an identical

(26) Gubelmann, M. H.; Williams, A. F. The Structure and Reactivity of Dioxygen Complexes of the Transition Metals. In *Structure and Bonding*; VCH Publishers: Weinheim, FRG, 1984; p 1.

(27) (a) Svensson, I.-B.; Stomberg, R. *Acta. Chem. Scand.* **1971**, *25*, 898. (b) Drew, R. E.; Einstein, F. W. B. *Inorg. Chem.* **1972**, *11*, 1079; **1973**, *12*, 829. (c) Mimoun, H. In *The Chemistry of Peroxides*, Patai, S.; Ed.; Wiley Interscience: New York, 1983.

TABLE V: Total Energies, Some Overlap Populations of 23–30 and the Shortest O–H (H of DHF) Distance

	23	24	25	26	27	28	29	30
energy, eV	−1909.55	−1908.86	−1907.02	−1900.26	−1909.34	−1908.87	−1907.53	−1903.1
O–H, Å	2.33	2.07	2.00	1.68	2.35	2.09	2.02	1.70
overlap populations								
V–O[a]	0.478	0.477	0.484	0.494	0.264	0.276	0.270	0.273
O–O[b]	0.396	0.397	0.402	0.399	0.416	0.415	0.416	0.400
O–H	0.000	0.000	0.000	−0.145	0.000	0.000	−0.030	−0.027
C–H	0.825	0.825	0.826	0.829	0.825	0.826	0.852	0.684

[a] Oxygen of superoxo or peroxo (V–O 1.90 Å). [b] O–O 1.40 Å.

O–O separation in the two structures. A very flat minimum exists for the superoxo structure as a function of the bending angle, θ. The total energy is unchanged from 180° to ~150°. An angle of 90° is unfavorable by ~3 eV. The total energy of the peroxo form is only 0.5 eV higher than the superoxo form. An angle of 150° for **18** is applied in the rest of the study. Calculations on the superoxo structure with an O–O distance of 1.25 Å also reveal a favorable bending angle of ~150°.

For both coordination modes a decrease in the oxygen–oxygen overlap population is calculated upon adsorption, from 0.570 in O_2(g) to 0.395 and 0.413 for the η^1- and η^2-coordinated species, respectively. The vanadium to oxygen overlap population is highest in the peroxo structure.

The bond obtained between a η^2-coordinated dioxygen and $(VO)_2O_6^{8-}$ can be described as an interaction of the partly occupied π_z^* of O_2 and the unoccupied antibonding vanadium oxygen d_{xz} + p_x orbital, **21**. A gain of 0.12 electrons is calculated for d_{xz}. For the superoxo structure the σ bond of O_2 is involved in bonding too. A loss of 0.11 electrons from the σ orbital is computed. This electron density is mainly transferred to d_{z^2} (0.06 electrons gained overall) and p_z (0.08 electrons gained overall) of vanadium. Again, the π_z^* orbital of O_2 interacts with the antibonding d_{xz} oxygen p_x orbital, **22**.

21 22

Coadsorption of O_2(g) and DHF on the Vanadyl Pyrophosphate Surface. A Model for the Formation of Maleic Anhydride

Let us now outline a possible reaction path from the initially formed 2,5-dihydrofuran to maleic anhydride. For this purpose we will use a $V_2O_8^{8-}$ cluster as a model for the surface, as it was argued above that this is a good model for the vanadyl pyrophosphate surface.

The presence of two vanadium atoms, located 3.19 Å from each other, on the vanadyl pyrophosphate surface leads to a possible activation of O_2(g) at one of the vanadium atoms, while DHF remains adsorbed at the other vanadium atom. The are four main combinations of a η^1-superoxo adsorbed molecular oxygen and DHF as outlined in **23–26**. For the coadsorption of η^2-peroxo molecular oxygen and DHF another four main possible orientations of O_2 and DHF emerge, as shown in **27–30**.

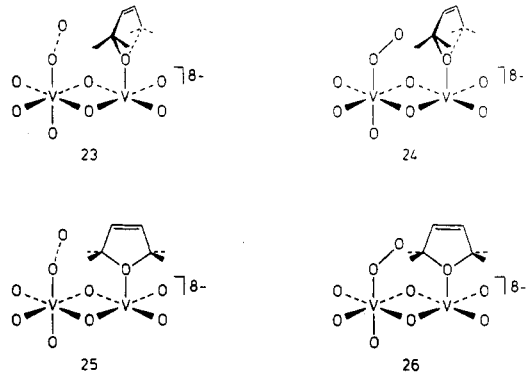

23 24 25 26

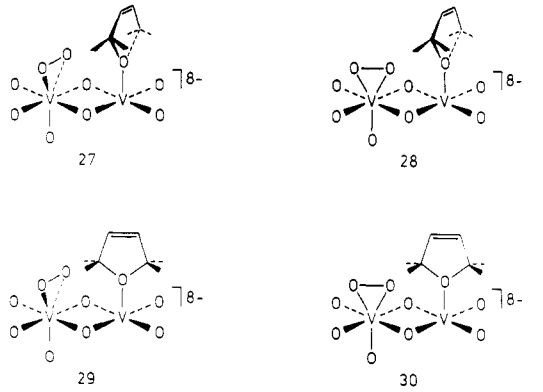

27 28 29 30

Table V gives the total energy and some overlap populations of interest for the present study.

It appears from Table V that the energy difference is only 0.21 eV between the most stable structure with η^1-superoxo molecular oxygen coadsorbed with DHF on the vanadyl pyrophosphate surface and the lowest energy structure of η^2-peroxo molecular oxygen and DHF on the surface. This indicates that within the present calculational method it is not possible to distinguish between these two lowest energy structures of adsorbed molecular oxygen and DHF. In two other pairs of geometries of molecular oxygen and DHF coadsorbed (**24** and **28**, and **25** and **29**) the difference in energy is also very small, whereas **26** is considerably higher in energy than **30**. The latter case is due to electronic/steric repulsion between the terminal oxygen and the two hydrogens in the 2-position of DHF. The different overlap populations are remarkably constant for the different orientations of either a η^1-superoxo or a η^2-peroxo molecular oxygen coadsorbed with DHF. The only two overlap populations that are different for the various orientations are O–H or C–H in **26** and **30**; a negative O–H overlap population is found in **26** and a decrease in the C–H overlap population is observed for **30**.

We will now proceed to a description of how maleic anhydride can be formed from coadsorbed molecular oxygen and DHF on the vanadyl pyrophosphate surface. We are aware of the fact that the quantitative results obtained by the extended Hückel calculations cannot be sufficiently trusted in studies where several bonds are simultaneously formed or cleaved. But, as our intention, here in this part of the paper, is to give a qualitative description of a possible reaction path, this method should be able to provide us with some useful trends. As a starting point for our analysis we will study the rotation of DHF coadsorbed with either a superoxo or a peroxo molecular oxygen around the axes outlined in a top view in **31** and **32**.

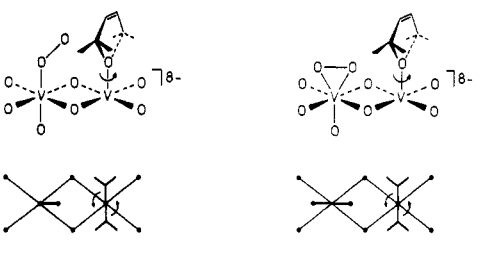

31 32

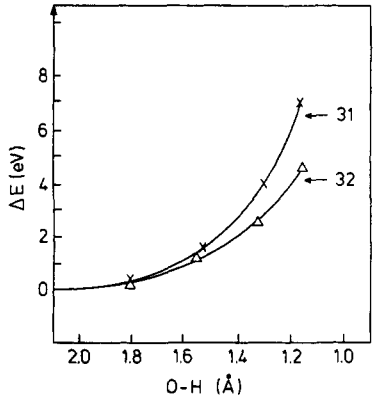

Figure 6. Variation in the total energy of **31** and **32** when rotating around the V–O (DHF) axis. The O–H distances is measured from the hydrogen in the 2-position of DHF to the nearest oxygen located at the adjacent vanadium atom.

When one of the two coadsorbed molecules on the vanadyl pyrophosphate surface is rotated, the terminal oxygen of a η^1-superoxo or one of the oxygens in a η^2-peroxo adsorbed molecular oxygen is brought close to the hydrogen of the C–H bond in the 2-position at DHF. These approaches of oxygen to hydrogen leads to several electronic changes.

In these rotations DHF starts out being oriented perpendicular to the V–V direction of the surface whereas the oxygen fragment, either superoxo or peroxo, stays fixed along the V–V direction (**31** and **32**). Figure 6 shows the changes in energy for the two different systems as a function of the O–H distance. The rotations shown correspond to rotation angles from 0° to 75° round the V–O (DHF) axis.

From Figure 6 it is seen that in the course of the rotation of DHF, when coadsorbed with a peroxo species (**32**), the approach of the hydrogen in DHF leads to an increase in energy. It costs about 4.6 eV to rotate. In the superoxo case (**31**) about 6.8 eV is required for the approach of the hydrogen to oxygen to the same O–H distance (1.15 Å), which indicates that the former is the least unfavorable. Besides the changes in energy several changes in bonding is also observed: For the rotation of **31** the C–H overlap population in DHF is reduced from 0.826 to 0.525, whereas the O–H overlap population increases from 0.000 to 0.209 over the range of O–H bond distances in Figure 6. This tells us that the C–H bond is weakened and that a O–H bond is made. The V–O (the oxygen which interacts with the hydrogen) overlap population in **32** is also affected by the rotation; it decreases from 0.281 to 0.234. In rotation **32** the C–H overlap population of DHF is also reduced from 0.826 to 0.286, whereas the O–H overlap population again shows an increase from 0.000 to 0.408 for the O–H bond distance changes of Figure 6. This also indicates a weakening of the C–H bond, and an O–H bond being formed too.

The change in nature of the C–H bond of DHF and of the interaction between an oxygen from the peroxo fragment and hydrogen in DHF can be traced to a controlling orbital interaction; the σ_{C-H} donates electron density into the σ^*_{O-O} orbital which is the LUMO as shown in **33**. The σ_{C-H} orbital donates 0.3 electrons

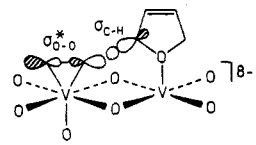

33

into the σ^*_{O-O} orbital by this interaction.

The donation of electron density from the σ_{C-H} orbital into the σ^*_{O-O} orbital thus leads to the weakening/cleavage of the C–H bond and the formation of an O–H bond. A similar type of C–H activation has also been found in the reactions of several types of transition-metal peroxo complexes;[28] in the case of transition-metal peroxo complexes the reaction with, e.g., benzene leads to a hydroxylation reaction.[28]

The first step of this proposed mechanism causes a hydrogen transfer from the 2-position in DHF to, probably, one of the oxygens of a coadsorbed η^2-peroxo oxygen fragment, although we cannot, on the basis of these calculations, exclude the η^1-superoxo species being active in the process. When an oxygen from the η^2-peroxo species interacts with the hydrogen the observed decrease in overlap population for the V–O bond (O from η^2-peroxo) might indicate that this bond will break by the hydrogen-transfer reaction, leading to a η^1-coordinated O–O–H as shown in **34**. The

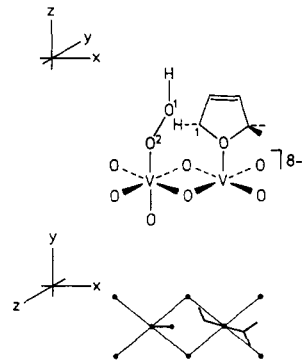

34

same intermediate is also formed in the case of an interaction between a η^1-superoxo dioxygen coadsorbed with DHF.

Calculation of the preferred orientation of the O–H group in **34** shows that an orientation with the hydrogen pointing in the z direction is 0.24 eV more favorable than the one where the hydrogen points in the opposite direction. With **34** as intermediate on the reaction path the formation of the 2-hydroxy derivative of DHF is a feasible process. The orientation of DHF, for which the hydrogen is transferred to the oxygen, is also the optimum position for interaction between O^1 and C^1 of **34**. In this position the C^1–O^1 overlap population is 0.635 (C^1–O^1 distance 1.60 Å), showing that significant C–O bonding is present. If the DHF derivative in **34** is rotated away from this optimum position (where the DHF derivative is rotated 15° away from the V–V direction) to, e.g., a position where the DHF derivative is oriented perpendicular to this direction, the energy required for bringing it back to the optimum position is less than 2 eV. Besides the formation of a C–O bond the O^1–O^2 overlap population is also reduced slightly when C^1 and O^1 interact. With the DHF derivative oriented perpendicular to the V–V direction the O^1–O^2 overlap population is 0.420, and 0.401 in the position where the optimum interaction between C^1 and O^1 occurs (**34**). The process described here gives then the 2-hydroxy derivative of DHF (2HDHF) and an adjacent V–O function on the surface, **35**.

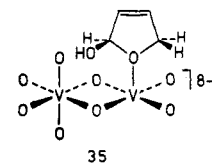

35

The above description of the formation of **35** is a two-step process, but we cannot exclude a one-step process, an "attachment–insertion" reaction similar to the one suggested for the hydroxylation of C–H bonds by oxene-like reagents.[29]

Let us now try to outline a possible path for the formation of maleic anhydride from 2HDHF and the neighboring vanadyl group. We will only consider one way which from energetics and bonding pictures shows to be fairly reasonable, although the results presented in the following cannot exclude other reaction paths.

(28) See e.g.: Bonchio, M.; Conte, V.; Di Furia, F.; Modena, G. *J. Org. Chem.* **1989**, *54*, 4368.

(29) Korzekwa, K.; Trager, W.; Gouterman, M.; Spangler, D.; Loew, G. *J. Am. Chem. Soc.* **1985**, *107*, 4273.

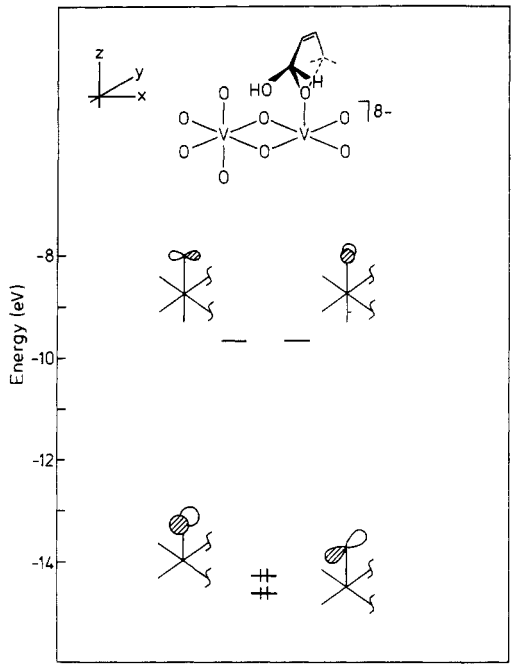

Figure 7. The frontier orbitals of the vanadium–oxygen bond in **35**.

The presence of the V–O function adjacent to 2HDHF is also important for the further reaction. The V–O function is located in an optimum position for interaction with the hydroxy function in 2HDHF, leading to the asymmetric unsaturated lactone. The electronic structure of the V–O function can be established from the frontier orbitals shown in Figure 7.

Figure 7 shows that the V–O function contributes to the frontier orbitals with low-lying unoccupied as well as with relatively high-lying occupied molecular orbitals of p_x, p_y, and p_z character. These orbitals then have the possibility of interacting with either the O–H or C–H bond in 2HDHF by accepting or donating electron density. The interaction of the O–H and the C–H bond in 2HDHF is analyzed as a function of the rotation angle of 2HDHF, going from −30° to +30°, as shown in **36**, in an attempt to elucidate the next step in the formation of the asymmetric unsaturated lactone.

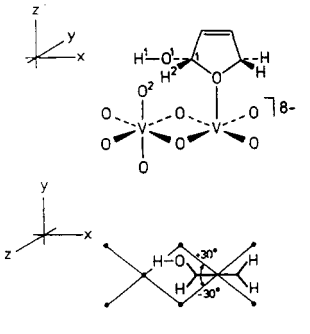

36

In the rotation sketched in **36**, the shortest H^1–O^2 distance is 1.17 Å and the shortest H^2–O^2 is 1.61 Å, indicating that the best interaction between 2HDHF and the oxygen on the adjacent vanadium atom is the interaction of O^2 with the H^1 of the hydroxyl group of 2HDHF. The total energy of the system rises by about 2 eV upon a rotation of +30°. Several electronic changes takes place upon rotation: The H^1–O^2 distance is 1.78 Å in the starting position with the following overlap populations: C^1–O^1 0.601, O^1–H^1 0.603, and H^1–O^2 −0.02; in the position with the shortest H^1–O^2 distances (1.17 Å) these overlap populations have changed to 0.633, 0.366, and 0.154, respectively. These results show that, when the C^1–O^1 bond increases in strength, meaning that the C=O bond is beginning to form, the O^1–H^1 bond is weakened and a H^1–O^2 bond is being formed. The formation of H^1–O^2 bond can be traced to interaction between the second HOMO shown in Figure 7 and the σ^*_{O-H} in the hydroxyl group in 2HDHF.

By the reaction path presented so far we are now near the end of the reaction, for we have reached a hydroxy group at the adjacent vanadium atom and a 2HDHF radical-like species coordinated to the other vanadium atom, as shown in **37**. With

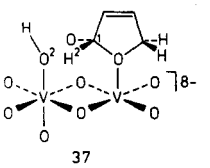

37

an orientation of the system as depicted in **37**, the last step in the formation of the asymmetric unsaturated lactone is an abstraction and a transfer of H^2 to O^2, and a rehybridization of C^1 from sp^3 to sp^2. The H^2–O^2 distance in **37**, with the bond lengths and angles used here for the adsorbed species (see Appendix), is calculated to be 1.61 Å, and for this distance a small H^2–O^2 overlap population is observed (0.06), indicating that a hydrogen transfer might be possible. This transfer of H^2 to O^2, under formation of H_2O and the asymmetric unsaturated lactone, **38**, leads to a decrease in the total energy of the system by 0.87 eV, also indicating that this process seems possible.

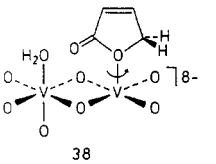

38

By the process described so far DHF has by use of one molecule of oxygen been oxidized to the asymmetric unsaturated lactone and a water molecule on the vanadyl pyrophosphate surface. The next step in the formation of maleic anhydride on the vanadyl pyrophosphate surface is an exchange of the water molecule with molecular oxygen in **38** and a rotation of the asymmetric unsaturated lactone by 180°. This would lead another CH_2 group to be near the newly adsorbed and activated molecular dioxygen at the adjacent vanadium atom. The formation of maleic anhydride can thus take place in a way similar to that described above for the formation the asymmetric unsaturated lactone. The present results seem to support the observation by Busca and Centi that the lower reaction path of Scheme I represents a likely path for the formation of maleic anhydride on a vanadyl pyrophosphate surface.

Conclusion

In this study we have analyzed the electronic structure of the vanadyl pyrophosphate surface trying to explain some of the steps involved in the transformation of *n*-butane to maleic anhydride catalyzed by this surface using molecular oxygen as the oxygen donor. First, an electrophilic oxygen from a surface vanadyl group can insert in the 1,4-positions of butadiene in a concerted [2+-4]-like cycloaddition process. The thereby formed 2,5-dihydrofuran fragment rearranges itself to a "vertical" position where it can interact with a neighboring adsorbed dioxygen species.

The nature of this dioxygen fragment when adsorbed on a clean vanadyl pyrophosphate surface was analyzed. The two coordination modes, η^1 (Θ = 150°) and η^2, gave quite similar results, so a definite assignment of the geometry could not be made. When interacting with a coadsorbed DHF molecule the η^2-peroxo form seems to provide the most likely structure of the dioxygen part, but the η^1-superoxo possibility cannot be excluded. Both dioxygen structures upon abstraction of an 2-hydrogen from DHF lead to an O–O–H surface species. This species can transfer an OH group to the DHF radical derivative forming a new vanadyl group. The newly formed hydroxylated DHF can eliminate water upon reaction with the new neighboring vanadyl oxygen leaving back, on the surface, the asymmetric unsaturated lactone. Another molecule of O_2 can undergo exactly the same reaction sequence with the 5-position of the lactone. More detailed mechanistic

TABLE VI: Atomic Parameters

atom	orbital	H_{ii}, eV	ξ_1	ξ_2	c_1[a]	c_2[a]
V	4s	-8.81	1.30			
	4p	-5.52	1.30			
	3d	-11.00	4.75	1.70	0.4755	0.7052
O	2s	-32.20	2.28			
	2p	-14.80	2.28			
C	2s	-21.40	1.63			
	2p	-11.40	1.63			
H	1s	-13.60	1.30			

[a] Coefficients used in the double zeta expansion of the metal d-orbitals.

studies of these later steps of the proposed reaction path will definitely be of great interest.

Acknowledgment. B.S. is thankful to the Carlsberg Foundation for economical support and to Thanks to Scandinavia, Inc. (especially Mr. Richard Netter) for making the stay at Cornell possible. We are thankful to Arne Lindahl for his careful preparation of the drawings and to Susan Jansen for sending a paper prior to publication.

Appendix

The extended Hückel[19] molecular and tight binding[20] approach is applied throughout this study. Bond distances and angles for the different surface models are taken as average of the experimental values reported for the vanadyl pyrophosphate structure.[12] This leads to a V-V distance of 3.188 Å and a V=O distance of 1.628 Å. The geometry of 2,5-dihydrofuran is in accordance with the experimentally reported structure.[30] Butadiene has C-C separations of 1.48 and 1.34 Å and all angles are 120°.[31] The dioxygen species have an O-O distance of 1.40 Å.[26] The distance between vanadium and an oxygen from the adsorbed dioxygen is 1.90 Å.[25] Atomic parameters are listed in Table VI. In the tight-binding calculations, properties averaged over the Brillouin zone were estimated by the use of a 10 k-point set according to the geometrical method by Ramirez and Böhm.[32]

(30) Courtieu, J.; Gounelle, Y. *Mol. Phys.* **1974**, *28*, 161.
(31) March, J. *Advanced Organic Chemistry*, 3rd ed.; Wiley Interscience: New York, 1985; p 19.
(32) Ramirez, R.; Böhm, M. C. *Int. J. Quantum Chem.* **1986**, *30*, 391.

A Charge-Iterative Hamiltonian for Molecular Electronic Spectra

John David Baker and Michael C. Zerner*

Quantum Theory Project, University of Florida, Gainesville, Florida 32611 *(Received: June 19, 1990)*

A complete charge-dependent INDO model Hamiltonian appropriate for the calculation of molecular spectra is developed and examined. A procedure for the acquisition of atomic and molecular parameters is presented that makes use of readily available experimental data. Simplified parameter functions, allowing more information to be incorporated into the model with less effort than is the case for previous parametrization strategies, are suggested. The charge-iterative model forwarded here surpasses the current spectroscopic INDO Hamiltonian in the quantitative prediction of n-π^* excitation energies for carbonyls without loss of accuracy in the prediction of π-π^* excitation energies.

I. Introduction

Semiempirical Hamiltonians for electronic structure calculations owe their efficiencies to reducing the number of integrals processed to N^2, where N is the size of the basis set. In so doing, matrix multiplications and diagonalizations, both N^3 steps, dominate, at least at the Hartree-Fock (HF) level. In addition, most semiempirical methods utilize a minimum basis set (MBS) of valence-type orbitals, further reducing N in the more complex N^3 steps. These models compensate for the reduction of integrals and small basis sets by parametrizing directly on atomic phenomena and molecular properties, and are thus often able to reproduce experimental values in a more accurate fashion than the MBS ab initio calculations on which they are modeled.[1,2]

The MBS assumption is definitely a restriction, as it does not properly allow the orbitals associated with an atom in a molecule to expand or contract with gain or loss of electrons, and more or less freezes the potential of an atom in a molecule to that seen in neutral atoms.

In this paper, we reexamine the atomic parameters that enter into most semiempirical Hamiltonians, borrowing from concepts that seem natural in density functional theory.[3] Density functional theory suggests atomic parameters that are functions of charge and atomic number. We present an initial attempt at utilizing such parameters in a fashion appropriate for the calculation of electronic excitations and ionizations. Due to the success of the spectroscopic version of the intermediate neglect of differential overlap (INDO/S) approximation in the prediction of electronic properties, we seek to extend the basic form of this Hamiltonian.[4]

At the heart of many semiempirical models is the determination of purely atomic parameters from experimental atomic information. These atomic parameters, in turn, help define the atomic potentials that electrons in the molecule realize.

We expand the total atomic energy (E) in a Taylor series with respect to the total number of electrons N

$$E(N,Z) = E(Z,Z) + (N-Z)\frac{\partial E}{\partial N} + \tfrac{1}{2}(N-Z)^2\frac{\partial^2 E}{\partial N^2} + \text{higher terms} \quad (1)$$

and utilize the concepts of hardness[5] and electronegativity or chemical potential[6,7]

$$\text{hardness} = \eta \equiv \tfrac{1}{2}\left(\frac{\partial^2 E}{\partial N^2}\right) \quad (2)$$

$$\text{electronegativity} = \chi \equiv -\frac{\partial E}{\partial N} = -\text{chemical potential} \quad (3)$$

(1) Sadlej, J. *Semi-Empirical Methods of Quantum Chemistry*; Wiley: New York, 1985.
(2) Pople, J. A.; Beveridge, D. L. *Approximate Molecular Orbital Theory*; McGraw-Hill: New York, 1970.
(3) Parr, R. G.; Yang, W. *Density-Functional Theory of Atoms and Molecules*; Oxford: New York, 1989.
(4) Ridley, J.; Zerner, M. *Theor. Chim. Acta* **1973**, *32*, 111-134.
(5) Pearson, R. G. *J. Chem. Ed.* **1987**, *64*, 561-567.
(6) Pritchard, H. O.; Skinner, H. A. *Chem. Rev.* **1955**, *55*, 745-786.

0022-3654/91/2095-2307$02.50/0